Pressure induced second-order structural transition in $Sr_3Ir_2O_7$

2014 J. Phys.: Condens. Matter 26 215402

(http://iopscience.iop.org/0953-8984/26/21/215402)

IOP Publishing Journal of Physics: Condensed Matter
J. Phys.: Condens. Matter **26** (2014) 215402 (5pp) doi:10.1088/0953-8984/26/21/215402

Pressure induced second-order structural transition in $Sr_3Ir_2O_7$

Z Zhao[1,2], S Wang[2,3], T F Qi[4], Q Zeng[2,3], S Hirai[3], P P Kong[5], L Li[4], C Park[6], S J Yuan[4,7], C Q Jin[5], G Cao[4] and W L Mao[2,3]

[1] Department of Physics, Stanford University, Stanford, CA 94305, USA
[2] Photon Science and Stanford Institute for Materials and Energy Sciences, SLAC National Accelerator Laboratory, Menlo Park, CA 94025, USA
[3] Department of Geological and Environmental Sciences, Stanford University, Stanford, CA 94305, USA
[4] Center for Advanced Materials, Department of Physics and Astronomy, University of Kentucky, Lexington, Kentucky 40506, USA
[5] Institute of Physics, Chinese Academy of Sciences, Beijing, People's Republic of China
[6] High Pressure Collaborative Access Team, Geophysical Laboratory, Carnegie Institution of Washington, Argonne, IL 60439, USA
[7] Department of Physics, Shanghai University, Shanghai, People's Republic of China

Email: zhaozhao@stanford.edu

Received 22 January 2014, revised 16 March 2014
Accepted for publication 24 March 2014
Published 8 May 2014

Abstract

We conducted *in situ* angle dispersive high pressure x-ray diffraction experiments on $Sr_3Ir_2O_7$ up to 23.1 GPa at 25 K with neon as the pressure transmitting medium. Pressure induces a highly anisotropic compressional behavior seen where the tetragonal plane is compressed much faster than the perpendicular direction. By analyzing different aspects of the diffraction data, a second-order structural transition is observed at approximately 14 GPa, which is accompanied by the insulating state to nearly metallic state at 13.2 GPa observed previously (Li *et al* 2013 *Phys. Rev.* B **87** 235127). Our results highlight the coupling between electronic state and lattice structure in $Sr_3Ir_2O_7$ under pressure.

Keywords: high pressure, structural transition, iridate

S Online supplementary data available from stacks.iop.org/J.PhysCM/26/215402/mmedia

(Some figures may appear in colour only in the online journal)

1. Introduction

The double-layered iridate $Sr_3Ir_2O_7$ belongs to the Ruddlesden–Popper series $Sr_{n+1}Ir_nO_{3n+1}$ ($n = 1$, 2 and ∞), where n represents the number of Ir–O layers in a unit cell [1–5]. In $Sr_{n+1}Ir_nO_{3n+1}$, there is a strong spin–orbit interaction that competes with the Coulomb repulsion, crystal field, and other relevant energies [3–15]. For $n = 1$, Sr_2IrO_4 is the archetype $J_{eff} = 1/2$ insulator with an anisotropic antiferromagnetic ground state [3, 4, 9, 10, 12, 13]. For $n = \infty$, $SrIrO_3$ is a correlated metal showing three-dimensional physical properties [11]. Intermediate between $n = 1$ and ∞, lies $n = 2$ $Sr_3Ir_2O_7$, a $J_{eff} = 1/2$ Mott insulator in the vicinity of a metal to insulator transition. Therefore, $Sr_3Ir_2O_7$ is sensitive to small perturbations in applied magnetic field, temperature, and chemical doping [5–7, 9, 14–16].

Pressure is a powerful tool for tuning interatomic distances and altering atomic arrangements. For materials with competing ground states, application of pressure has the potential for effectively tuning ground state, and possibly inducing novel phenomena. Layered iridates and ruthenates are among good examples. Ca_2RuO_4 experiences a first-order structural transition from the Mott insulating phase to a ferromagnetic metallic phase at 0.5 GPa, then transforms to another higher symmetry ferromagnetic metallic phase at around 5.5 GPa via a second-order structural transition [17–19]. $Ca_3Ru_2O_7$ undergoes a pressure-induced collapse of the antiferromagnetic orbital order at around 5.5 GPa, due to the suppression of RuO_6 octahedral distortions [20]. Sr_2IrO_4 experiences a magnetic transition around 17 GPa without any associated structural transition [21]. For $Sr_3Ir_2O_7$, two pressure and temperature dependent

electrical resistivity studies have been recently reported. In one study, pressure was increased up to 35 GPa at small pressure steps (~1.5 GPa) with hexagonal boron nitride (BN) powder as the pressure medium [16], and in the other study the pressure was increased to over 100 GPa without a pressure medium at relatively large pressure steps [22]. It was observed in both experiments that up to ~ 30 GPa there was a decrease of about four orders of magnitude in low temperature resistivity. Also, an insulating to nearly metallic transition was observed at a critical pressure of 13.2 GPa in the data set using smaller steps [16].

To explore structural behavior of $Sr_3Ir_2O_7$ under pressure, we performed new *in situ* angle dispersive high-pressure x-ray diffraction (XRD) experiments at 25 K up to 23.1 GPa. We present evidence for a pressure induced second-order structural transition occurring near 14 GPa. We also present and discuss the strong electron-lattice coupling and its implications for physical properties in $Sr_3Ir_2O_7$.

2. Experimental details

The samples used for the XRD experiment were synthesized by the method described in previous studies [5, 10, 13, 23, 24]. A symmetric diamond anvil cell (DAC) with 300 μm culet size was used. A tungsten gasket was pre-indented to a thickness of about 60 μm, and a 120 μm diameter sample chamber was drilled in the center. Ruby was used for determining pressure and neon was used as the pressure transmitting medium. *In situ* angle dispersive XRD data was collected at 16 BM-D at the advanced photon source (APS), Argonne National Laboratory (ANL). A gas membrane was used to increase pressure in the cryostat. The diffraction images were collected using a MAR345 detector and the 2-D diffraction images were integrated by using the program fit2D [25]. The Rietveld fitting on integrated powder diffraction pattern was performed by GSAS and the EXPGUI package [26]. Representative MAR3450 files and Rietveld profiles are presented in supplementary material figures S1 and S2 (stacks.iop.org/J.PhysCM/26/215402/mmedia).

3. Results and discussion

There has been a debate as to whether the ambient crystal structure of $Sr_3Ir_2O_7$ has the *I4/mmm* [27] or the *Bbcb* [5, 28] space group, where the lower symmetry orthorhombic *Bbcb* structure is regarded as a supercell with $\sqrt{2}a \times c$ (a and c are the lattice parameters for the smaller tetragonal *I4/mmm* cell). Recent results (including ours) of single-crystal XRD studies favor the *I4/mmm* structural model [14, 16]. As shown in figures 1(*a*) and (*b*), the double-layered perovskite tetragonal *I4/mmm* structure features random positions of the oxygen atoms in the tetragonal *a*–*b* plane and rotations of the IrO_6 octahedra. Previous studies indicate that the rotation of the IrO_6 octahedra correlates with the AFM ground state [1, 5, 12].

Representative XRD patterns collected at 25 K during compression are shown figure 1(*c*). All diffraction peaks from the sample shifted continuously to larger 2θ, and no first-order structural transition was observed over the entire

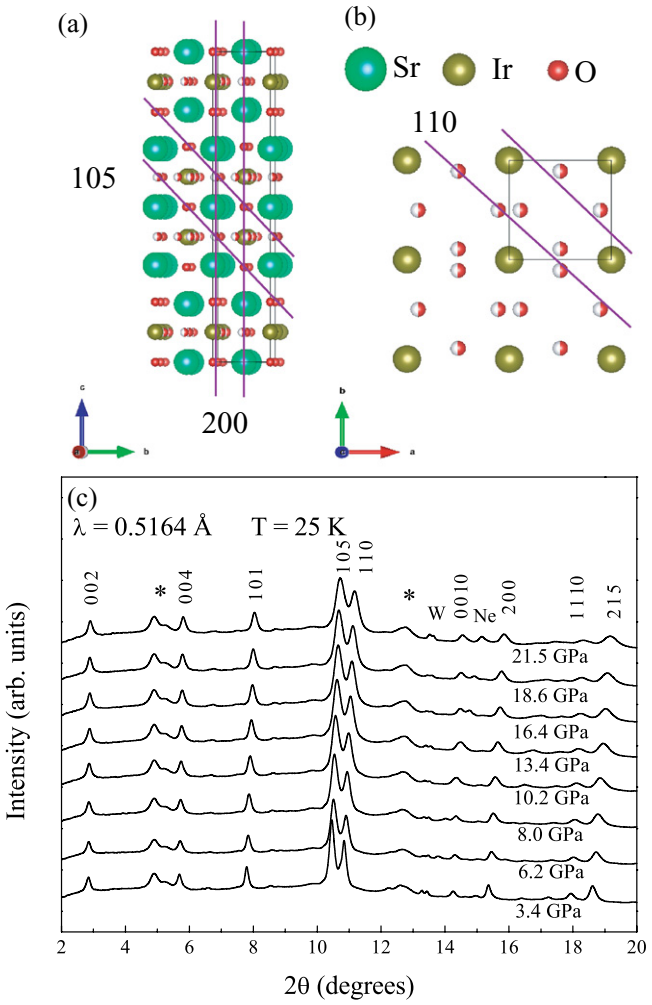

Figure 1. (*a*) and (*b*) Views of $Sr_3Ir_2O_7$ on *b*–*c* and *a*–*b* planes respectively, half red, half white, O sites are 50% occupied. (*c*) Representative XRD patterns collected at 25 K during compression. The peaks at 4.5–5.5 degrees and 12–13 degrees that do not shift with pressure are marked by asterisks and come from the cryostat.

pressure range studied. We first fit the well separated and intense peaks (0 0 2), (0 0 4) (0 0 10), (1 0 5), (1 0 1), (1 1 0) and (2 0 0), together with neon (1 1 1), with Voigt area functions by PEAKFIT. Figure 2 shows the linear fittings for the normalized *d*-spacings below and above 14 GPa. When we extrapolate the linear fit from below 14 GPa to higher pressure, they increasingly deviate from the experimental data indicating a change in compressibility. The transition can also be confirmed by monitoring the normalized cell parameters, the *c*/*a* ratio, and EOS fitting discussed below, and thus the pressure of the second-order structural transition is assigned to about 14 GPa. In addition, the peaks involving the *a* axis have comparatively larger width increases than those mainly involving the *c* axis, which may be explained by the fact that the random oxygen sites (50% occupancy sites) tend to have wider distributions upon compression.

Normalized cell parameters and the *c*/*a* ratio as a function of pressure are shown in figure 3 (cell parameters obtained from Rietveld refinements are given in table S2 of the supplementary material (stacks.iop.org/J.PhysCM/26/215402/mmedia)). The a/a_0 and c/c_0 below 14 GPa can be well

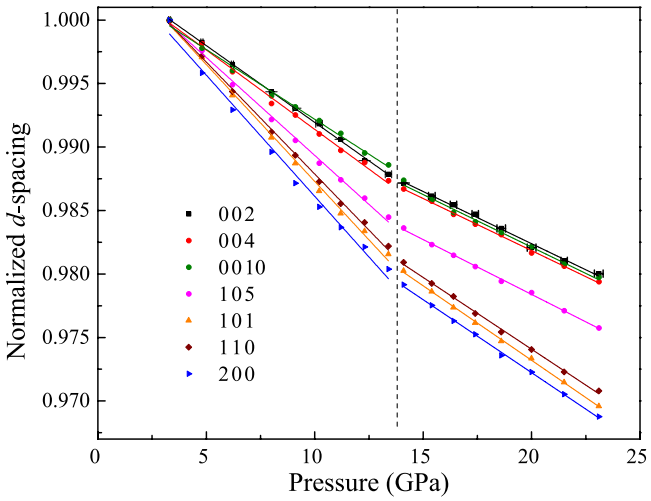

Figure 2. Evolution of normalized peak *d*-spacings with pressure, d_0 is the value at 3.3 GPa. Uncertainty in pressure is set to be half the absolute difference of the pressure measured before and after the diffraction measurement, and the uncertainty of the normalized *d*-spacing is smaller than marker size.

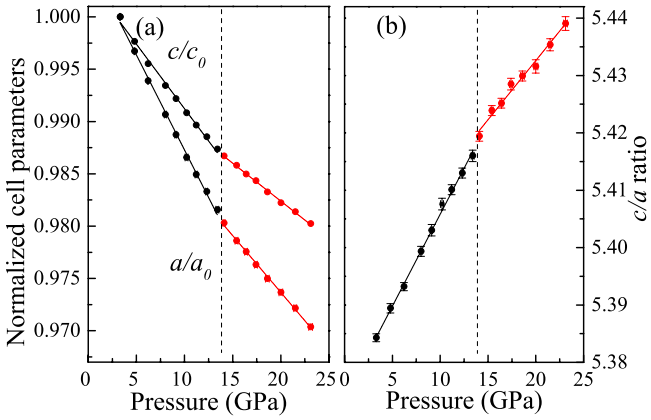

Figure 3. (*a*) Normalized cell parameters and (*b*) *c*/*a* ratio as a function of pressure. a_0 and c_0 are the values at 3.3 GPa. Errors are given by GSAS–EXPGUI program. Solid lines are linear fits.

Table 1. Linear fitting results of d(a/a_0)/dP, d(c/c_0)/dP, and d(c/a)/dP for two regions.

	d(a/a_0)/dP	d(c/c_0)/dP	d(c/a)/dP
Region/Units	GPa^{-1}	GPa^{-1}	GPa
Below 14 GPa	−0.0018(1)	−0.0012(1)	0.0032(1)
Above 14 GPa	−0.0011(1)	−0.0007(1)	0.0021(1)

described by linear fits. If we extended these lines, the experimental data increasingly deviated from them, so the data above 14 GPa was fitted separately. The data shows a strong anisotropy in the *a* and *c* directions (table 1), where the *a* axis is compressed about 50 % faster than the *c* axis. Consistently, we can see from figure 2 that the normalized *d*-spacings of (002), (004), and (0010) decrease much more slowly than other peaks like the (110) and (200). The strong anisotropy results in an increase in the *c*/*a* ratio from about 5.38 at 3.3 GPa to 5.44 at 23.1 GPa. A similar but much smaller anisotropy in

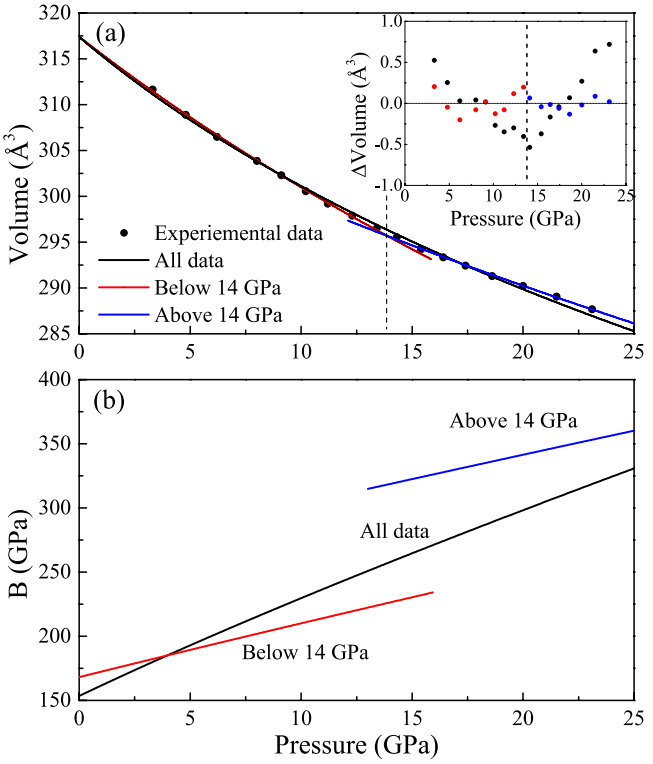

Figure 4. (*a*) Evolution of the unit cell volume with pressure and the EOS fitting results. Black dots are experimental data, and the error given by GSAS–EXPGUI is smaller than the marker size. The black, red, and blue curves are results attained by fitting all the data, only the data below 14 GPa, and only the data above 14 GPa respectively. The inset shows the difference between the volume from fitting and the experimental volume (V_{fit}–V_{exp}). (*b*) Evolution of incompressibility, $B = V \times dP/dV$, with pressure using different portions of the XRD data set.

compression was also observed in Sr_2IrO_4, as the *a* axis shrank about 20% faster than the *c* axis [21].

Figure 4(*a*) presents the EOS fitting results from the third-order BM EOS through EOSFIT [29], and the inset illustrates ΔV, the difference between experimental volume and calculated volume. We compare our fitting results with the other study on Sr_2IrO_4 [21] in table 2. For below 14 GPa and all data fittings, V_0 is fixed at 317.4 $Å^3$, which is based on temperature-dependent unit-cell volumes measured on the $Sr_3Ir_2O_7$ single crystal. For all the data, the fitting gives a relatively large pressure derivative of the bulk modulus $B' = 8.2(9)$ and a large VΔV especially above 14 GPa, indicating poor fitting, while fitting only the below 14 GPa data gives more reasonable values of $B' = 4.3(9)$. It becomes obvious that the fit below 14 GPa increasingly deviates from experimental data at higher pressure. A second-order BM EOS was used for above 14 GPa data, as limited by the number of data points, where it gives a comparatively small ΔV, see the inset of figure 4(*a*). Thus, we conclude that the second-order transition occurs at approximately 14 GPa. Figure 4(*b*) shows the evolution of incompressibility for the three fits: all the data, the data below 14 GPa, and the data above 14 GPa. It is reasonable that the 'all data' fitting curve falls in between the other two segment curves.

It is remarkable that a critical pressure of 13.2 GPa (see figure 5), that represents the insulating to nearly metallic

Table 2. Comparisons of fitted EOS parameters.

	EOS	Temperature	Pressure range	V_0	B_0	B'	Reference
Formula/Units		K	GPa	($Å^3$)	GPa	—	
Sr_2IrO_4	third-order BM	11	0 to 25 GPa	774 (2)	174 (5)	4.0(7)	[21]
$Sr_3Ir_2O_7$	third-order BM	25	0–25 GPa	317.4[a]	153(4)	8.2(9)	this study
	third-order BM		0–14 GPa	317.4[a]	168(4)	4.3(9)	
	second-order BM		14–25 GPa	310(1)	264(8)	4[a]	

[a] Indicates fixed value.

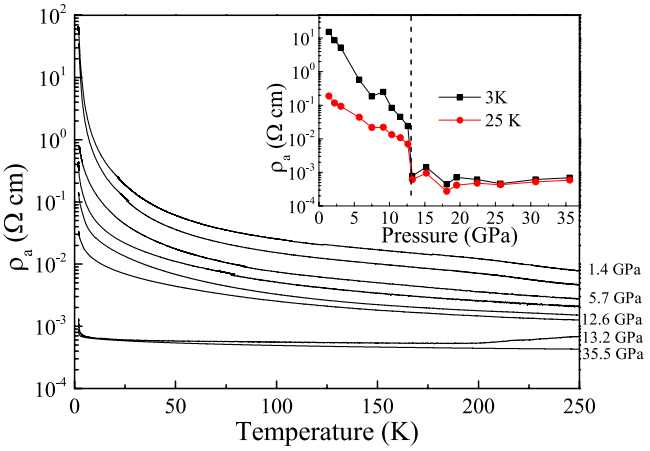

Figure 5. High pressure electrical transport data for a $Sr_3Ir_2O_7$ single crystal up to 35.5 GPa [16]. The inset shows the resistivity at 3 K and 25 K for all pressure points.

transition in single-crystal $Sr_3Ir_2O_7$, was observed under the more hydrostatic pressure [16]. The fact that the critical pressure for the electronic phase transition is reasonably close to 14 GPa for the structural phase transition provides evidence for correlations between the electronic state and crystal structure. Potential differences in pressure gradients and the deviatoric stress environment could affect the structural and electronic behavior. A systematic study using different pressure media is required for direct comparison of the conductivity and XRD results. In our XRD study, neon was used as the pressure medium and the pressure was monitored *in situ* at low temperature, while the pressure in the previous transport study was measured at room temperature with BN powder as the pressure medium [16]. For instance, in $Sr_3Ru_2O_7$, which also has a double layer perovskite structure, hydrostatic pressure up to 1.4 GPa maintained the paramagnetic state [30], while uniaxial pressure greater than 0.1 GPa induced a ferromagnetic order [31]. It is commonly known that for DACs, the pressure tends to increase due to clamping when temperature is lowered. Thus at 25 K, the pressure corresponding to the 13.2 GPa curve from the transport data could actually increase slightly (figure 5). In addition, the deviation from ideal stoichiometry may have a profound influence on the transition [32].

Pressure is a powerful means of tuning the balance between the strong spin–orbit interaction SOI, Coulomb repulsion U, crystal field and other interactions in $Sr_3Ir_2O_7$ [3, 4, 9, 10, 12, 13]. It is not surprising that our structural and transport results have similar transition pressures to show that the lattice and electronic state are strongly correlated. In terms of crystal structure under high pressure, the *c/a* ratio changes from 5.38 at 3.3 GPa to 5.44 at 23.1 GPa, and increases the interlayer bond distance to the intralayer bond distance ratio. Furthermore, the pronounced decrease of the tetragonal plane Ir–O bond distances and relative elongation of the *c* axis of IrO_6 octahedra will affect the Ir–O–Ir angle θ (figure 1(*b*)). For the electronic structure under pressure, the band widths generally increase. In the case of $Sr_3Ir_2O_7$, the J_{eff} = 1/2 and J_{eff} = 3/2 bands will increasingly mix with each other when compressed, which would tune the SOI [16, 21]. Indeed, changes in the crystal structure inevitably cause changes in the electronic structure, thus an electronic transition or vice versa, such as the transitions at 13.2 GPa in the electric resistivity and 14.1 GPa in the lattice. We need to point out that whether this second-order transition may involve a subtle change of space group (transition to a subgroup or a supergroup) is not differentiable by the powder XRD technique. Among layered ruthenates and iridates, the pressure induced second-order structural transition was only reported in Ca_2RuO_4 where *Pbca* phase II transformed into a higher symmetry *Bbcm* phase III with the disappearance of tilting of RuO_6 octahedra [17–19]. Obviously this is not the case with $Sr_3Ir_2O_7$: the high pressure phases II and III of Ca_2RuO_4 are both metallic while $Sr_3Ir_2O_7$ exhibits low temperature insulating behavior up to the highest pressure. No IrO_6 tilting but random rotations are found in $Sr_3Ir_2O_7$, in contrast to the ordered tilting and rotating in Ca_2RuO_4, and there lies an essential difference between 4*d* Ru^{3+} and 5*d* Ir^{3+}, the strong SOI in iridates that contributes to the strong coupling between lattice structure and electronic state.

To better illustrate the nature of the coupling, we can compare the similarities and differences between pressure and chemically doping in iridates. 5% La doping to Sr was found to increase the Ir–O–Ir bond angle θ from 154.922 to 156.034 degrees at 90 K and induce a fully metallic state [16]. For electron-doped $Sr_2IrO_{4-\delta}$ ($0 \le \delta \le 0.04$), the dilute oxygen vacancies increased the Ir–O–Ir angle from 156.280° (stoichiometric) to 157.078° (δ = 0.04) and induced a metallic behavior [32]. Theoretically, the change of θ can affect the superexchange interaction, where the electron hopping occurs via two t_{2g} orbitals at d_{xy} and d_{zx} for θ = 180° and for d_{xz} and d_{yz} at θ = 90° [33]. This suggests that applying external pressure could have a similar effect on increasing the bond angle and enhancing the itinerancy of electrons. However, compared with chemical doping, pressure may be a much less effective way to introduce a metallic state, as no itinerant electronic was observed up to 104 GPa [22]. Indeed, unlike chemical doping, pressure would neither introduce additional carriers that would shift the Fermi level (E_F), nor disorder scattering that may lead to bending of electronic bands.

These may explain the differences between the effects of chemical doping and pressure on $Sr_3Ir_2O_7$. And band structures calculations may provide important information about the evolution of the electronic states.

One interesting question is whether the second-order structural and electronic transition corresponds to any change in the magnetic order. For Sr_2IrO_4, pressure was found to eliminate the weak ferromagnetism at around 17 GPa without changing the low temperature insulating behavior [21]. The canted to collinear AFM transition (or a less likely paramagnetic-insulating transition) was driven by an increased crystal electric field [21]. In the case of $Sr_3Ir_2O_7$, different justifications are desirable to explain the dissimilar compressional behaviors between Sr_2IrO_4 and $Sr_3Ir_2O_7$, where the second-order structural transition and insulator to nearly metallic transition were only seen in $Sr_3Ir_2O_7$. Thus, how the spin–orbit interaction, Coulomb repulsion, crystal field, and long range magnetic order evolve under pressure, and what is the effect of the persistent randomness of IrO_6 *c* axis rotation await further calculations and spectroscopy experiments.

4. Conclusion

In summary, we have studied the structural behavior of $Sr_3Ir_2O_7$ under hydrostatic conditions at 25 K up to 23.1 GPa. A second-order structural transition was determined at 14 GPa by analyzing different aspects of the experimental XRD data. This transition occurs at a similar pressure to the insulating to nearly metallic transition at 13.2 GPa [16]. Our results highlight the coupling between the lattice and electronic state, a characteristic of the strong SOI in $Sr_3Ir_2O_7$.

Acknowledgment

We thank S Tkachev, C Kenney-Benson and H Yan for their technical support. The work at the University of Kentucky is supported by NSF through grants DMR-0856234, EPS-0814194 and DMR-1265162. Portions of the work are performed at HPCAT (Sector 16), APS, ANL. HPCAT operations are supported by DOE–NNSA under award no. DE-NA0001974 and DOE-BES under award no. DE-FG02-99ER45775, with partial instrumentation funding by NSF MRI-1126249. APS is supported by DOE–BES, under contract no. DE-AC02-06CH11357. ZZ, QZ and SH are supported by SIMES, Stanford Institute for Materials and Energy Sciences, funded by DOE–BES, Materials Sciences and Engineering Division, under contract DE-AC02-76SF00515. SW is supported by EFree, an Energy Frontier Research Center funded by the US DOE–BES, under award number DE-SG0001057.

References

[1] Huang Q, Soubeyroux J L, Chmaissem O, Sora I N, Santoro A, Cava R J, Krajewski J J and Peck W F Jr 1994 *J. Solid State Chem.* **112** 355–61
[2] Cava R J, Batlogg B, Kiyono K, Takagi H, Krajewski J J, Peck W F Jr, Rupp L W Jr and Chen C H 1994 *Phys. Rev.* B **49** 890–4
[3] Cao G, Bolivar J, McCall S, Crow J E and Guertin R P 1998 *Phys. Rev.* B **57** R11039
[4] Crawford M K, Subramanian M A, Harlow R L, Fernandez-Baca J A, Wang Z R and Johnston D C 1994 *Phys. Rev.* B **49** 9198–201
[5] Cao G, Xin Y, Alexander C S, Crow J E, Schlottmann P, Crawford M K, Harlow R L and Marshall W 2002 *Phys. Rev.* B **66** 214412
[6] Wojek B M and Berntsen M H 2012 *J. Phys.: Condens. Matter* **24** 415602
[7] Nagai I, Yoshida Y, Ikeda S I, Matsuhata H, Kito H and Kosaka M 2007 *J. Phys.: Condens. Matter* **19** 136214
[8] Clancy J, Plumb K and Nelson C 2012 arXiv:1207.0960v1
[9] Wojek B M, Berntsen M H, Boseggia S, Boothroyd A T, Prabhakaran D, McMorrow D F, Rønnow H M, Chang J and Tjernberg O 2012 *J. Phys.: Condens. Matter* **24** 415602
[10] Kim B J *et al* 2008 *Phys. Rev. Lett.* **101** 076402
[11] Moon S J *et al* 2008 *Phys. Rev. Lett.* **101** 226402
[12] Ye F, Chi S, Chakoumakos B C, Fernandez-Baca J A, Qi T and Cao G 2013 *Phys. Rev.* B **87** 140406
[13] Chikara S, Korneta O, Crummett W, DeLong L E, Schlottmann P and Cao G 2009 *Phys. Rev.* B **80** 140407
[14] Boseggia S, Springell R, Walker H C, Boothroyd A T, Prabhakaran D, Wermeille D, Bouchenoire L, Collins S P and McMorrow D F 2012 *Phys. Rev.* B **85** 184432
[15] Boseggia S, Springell R, Walker H C, Boothroyd A T, Prabhakaran D, Collins S P and McMorrow D F 2012 *J. Phys.: Condens. Matter* **24** 312202
[16] Li L, Kong P P, Qi T F, Jin C Q, Yuan S J, Delong L E, Schlottmann P and Cao G 2013 *Phys. Rev.* B **87** 235127
[17] Nakamura F, Goko T, Ito M, Fujita T, Nakatsuji S, Fukazawa H, Maeno Y, Alireza P, Forsythe D and Julian S R 2002 *Phys. Rev.* B **65** 220402
[18] Snow C S, Cooper S L, Cao G, Crow J E, Fukazawa H, Nakatsuji S and Maeno Y 2002 *Phys. Rev. Lett.* **89** 226401
[19] Steffens P *et al* 2005 *Phys. Rev.* B **72** 094104
[20] Karpus J F, Snow C S, Gupta R, Barath H, Cooper S L and Cao G 2006 *Phys. Rev.* B **73** 134407
[21] Haskel D, Fabbris G, Zhernenkov M, Kong P P, Jin C Q, Cao G and van Veenendaal M 2012 *Phys. Rev. Lett.* **109** 027207
[22] Zocco D A, Hamlin J J, Kim B J, Jeffries J R, Weir S T, Vohra Y K, Allen J W and Maple M B 2013 arXiv: 1304.5864v1
[23] Ge M, Qi T F, Korneta O B, De Long D E, Schlottmann P, Crummett W P and Cao G 2011 *Phys. Rev.* B **84** 100402
[24] Lorenzo J E, Mazzoli C, Jaouen N, Detlefs C, Mannix D, Grenier S, Joly Y and Marin C 2008 *Phys. Rev. Lett.* **101** 226401
[25] Hammersley A P 1997 FIT2D: an introduction and overview ESRF Internal Report ESRF97HA02T
[26] Toby B H 2001 *J. Appl. Cryst.* **34** 210–3
[27] Subramanian M A, Crawford M K and Harlow R L 1994 *Mater. Res. Bull.* **29** 645–50
[28] Ikeda S-I, Shirakawa N, Yanagisawa T, Yoshida Y, Koikegami S, Koike S, Kosaka M and Uwatoko Y 2004 *J. Solid State Chem.* **177** 3776–83
[29] Angel R J *EosFit v5.2*
[30] Ikeda S-I, Shirakawa N, Yanagisawa T, Yoshida Y, Koikegami S, Koike S, Kosaka M and Uwatoko Y 2004 *J. Phys. Soc. Japan* **73** 1322–5
[31] Ikeda S-I, Shirakawa N, Koiwai S, Uchida A, Kosaka M and Uwatoko Y 2001 *Physica* C **364–5** 376–8
[32] Korneta O B, Qi T, Chikara S, Parkin S, De Long L E, Schlottmann P and Cao G 2010 *Phys. Rev.* B **82** 115117
[33] Jackeli G and Khaliullin G 2009 *Phys. Rev. Lett.* **102** 017205